Electronic Supplementary Material (ESI) for Physical Chemistry Chemical Physics.

Supporting information on:

Correcting the record: The dimers and trimers of *trans*-*N*-methylacetamide

Thomas Forsting[a], Hannes C. Gottschalk[a], Beppo Hartwig[a], Michel Mons[b], and Martin A. Suhm[a]

a Institut für Physikalische Chemie, Georg-August-Universität Göttingen, Tammannstr. 6, 37077 Göttingen, Germany

b LIDYL ; CEA, CNRS, Université Paris-Saclay, 91191 Gif-sur-Yvette, France

List of Figures

List of Tables

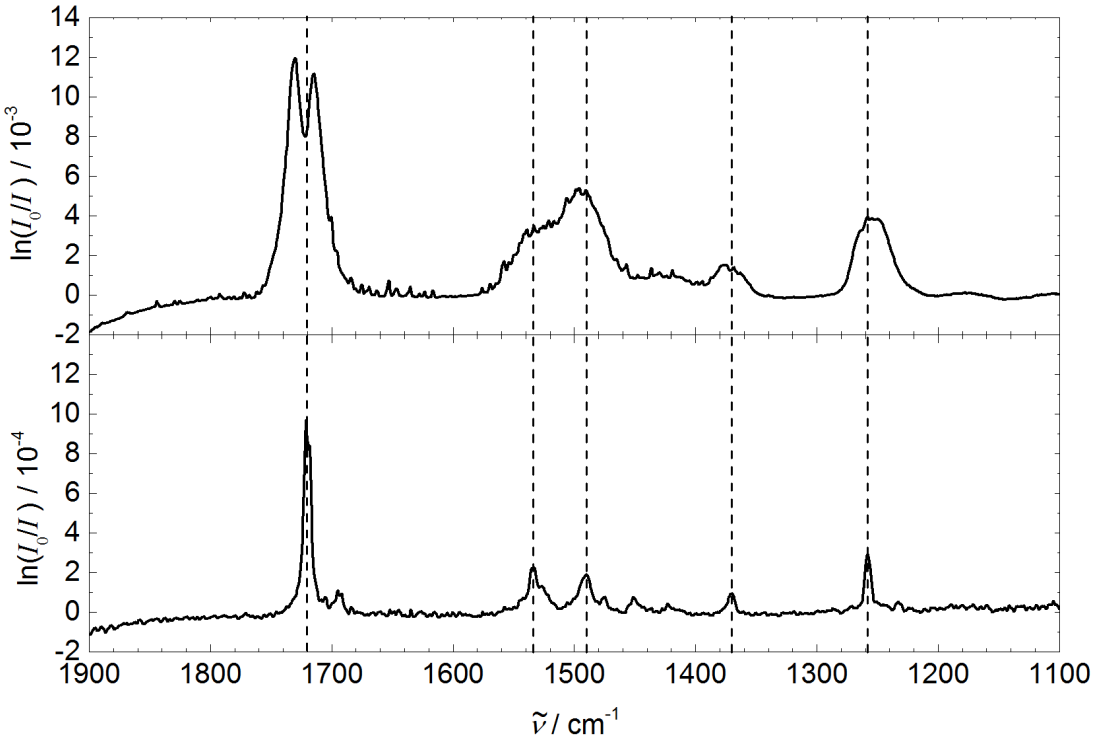

Fig. S1: Room temperature IR gas phase spectrum (top) and jet spectrum (bottom) of NMA diluted in He, between 1900 and 1100 cm^{-1}. Dashed vertical lines indicate the jet band maxima or dips, which correlate reasonably well with maxima or characteristic features in the gas phase spectra in this spectral range. Lines due to water ro-vibrational transitions confirm the correct wavenumber calibration within 0.2 cm^{-1}.
Experimental details: Globar | KBr beamsplitter and lenses | HgCdTe-detector.

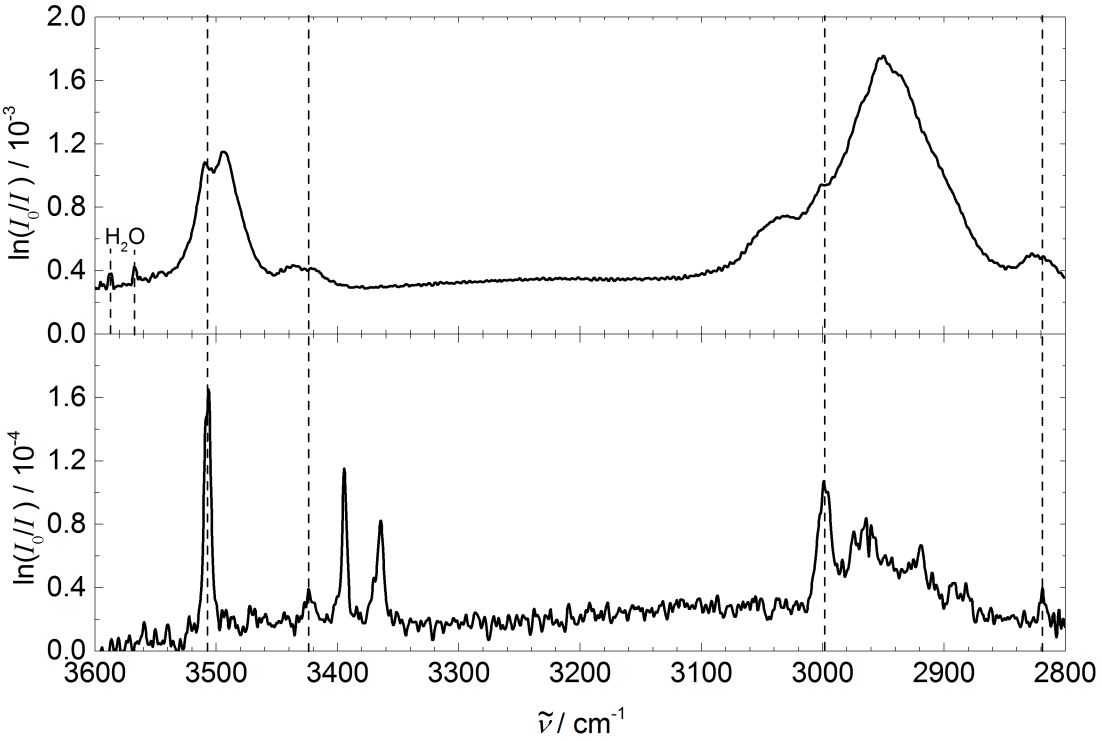

Fig. S2: Room temperature IR gas phase spectrum (top) and jet spectrum (bottom) of NMA diluted in He, between 3600 and 2800 cm^{-1}. Dashed vertical lines indicate some monomeric jet band maxima, which correlate only moderately well with maxima or characteristic features in the gas phase spectra in this spectral range, probably due to methyl torsional hot bands. The CH stretching region is very sensitive to temperature, as the comparison between jet and gas phase data suggests. The C=O stretching overtone is clearly revealed in the gas phase near 3425 cm^{-1}, in agreement with the weak jet spectral feature near 3420 cm^{-1}. Lines due to water ro-vibrational transitions confirm the correct wavenumber calibration within 0.2 cm^{-1}.
Experimental details: tungsten lamp (150 W) | CaF_2 beamsplitter and lenses | InSb-detector.

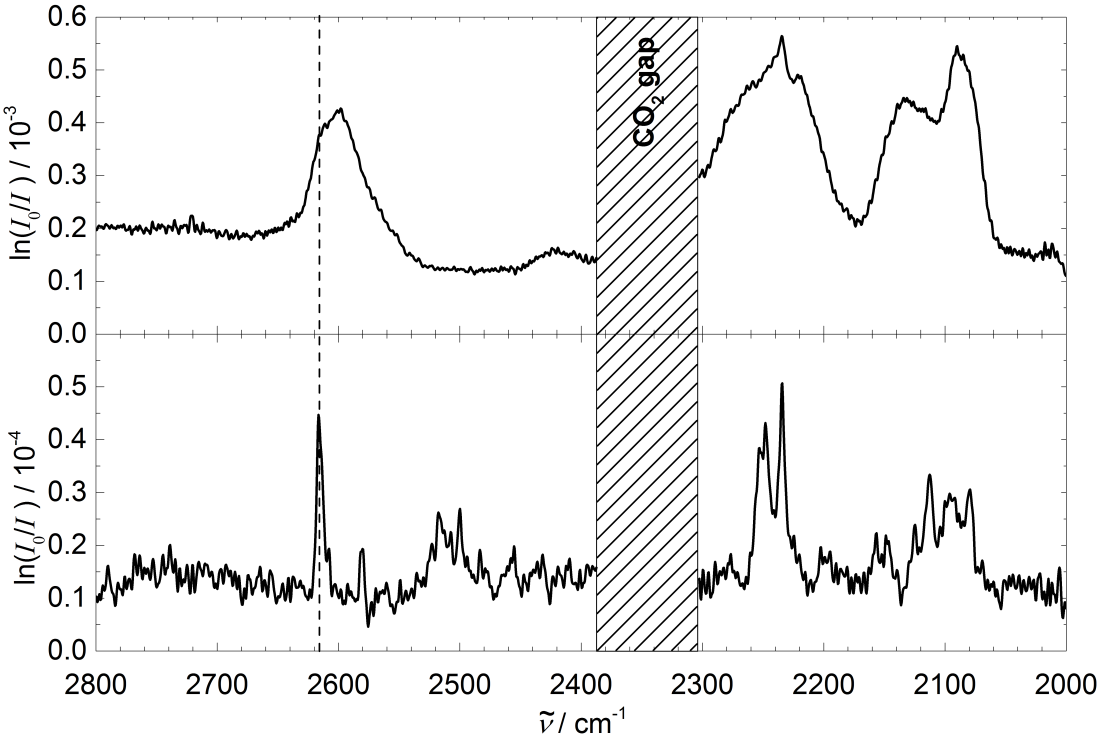

Fig. S3: Room temperature IR gas phase spectrum (top) and jet spectrum (bottom) of NMA-d_7 diluted in He, between 2800 and 2000 cm^{-1}. The CD stretching region is sensitive to temperature, as the comparison between jet and gas phase data suggests. The high IR absorption cross section of the asymmetric stretching band of CO_2 leads to spurious positive or negative signals between 2300 and 2390 cm^{-1} due to concentration fluctuations in the beam path between reference and sample measurements. Despite vaccum operation of the spectrometer and CO_2-depleted air purging of the narrow air gaps, these fluctuations exceed the statistical noise. Spectral intensities in this low transmission band would be distorted. Therefore the region marked as CO_2 gap is blanked out.

Experimental details: Globar | KBr beamsplitter and CaF_2 lenses | InSb-detector.

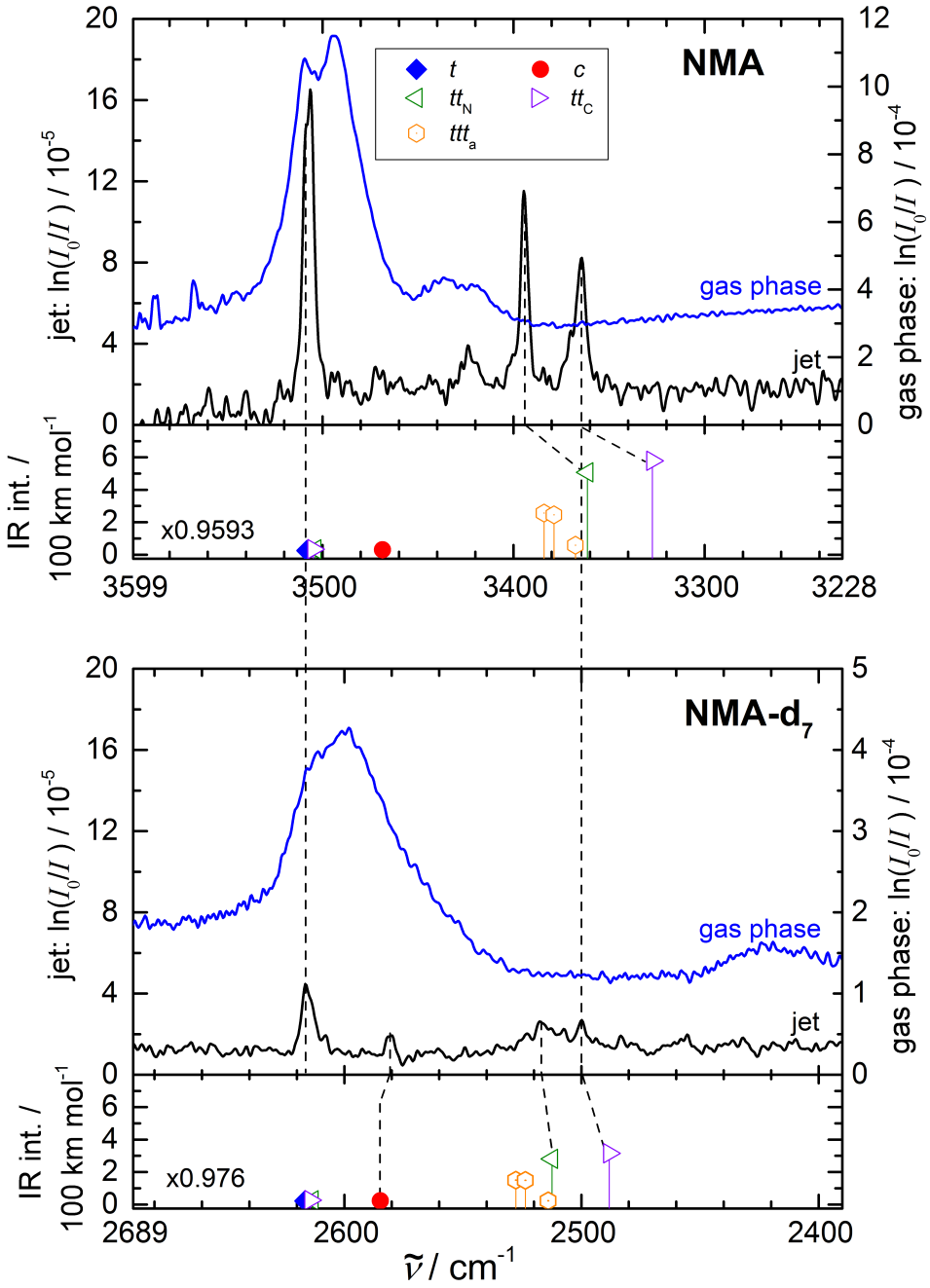

Fig. S4: Comparison of the experimental and harmonically predicted N−H/D stretching IR spectra of NMA (upper) with fully deuterated NMA-d_7 (lower panel) recorded under more diluted conditions. The N−D wavenumber scale is expanded by a factor of 1.235 and shifted such that the *trans* monomer (blue diamonds) and the most downshifted dimer peaks coincide (dashed vertical lines). Note the close correspondence of the weak *cis* monomer peaks (red circles), the missing monomer C=O overtone feature upon deuteration and the persistence of a second, less downshifted dimer peak, which rules out a Fermi resonance interpretation of the dimer doublet. The broad and shifted gas phase spectrum (blue) illustrates vibrational cooling in the jet. The harmonic dimer predictions (triangles) match somewhat better in the NMA-d_7 case after *trans* monomer scaling due to reduced anharmonicity in the deuterium bond. IR-active transitions for the strained, cyclic trimer (hexagons) may contribute in the less downshifted dimer range, as in the non-deuterated case.

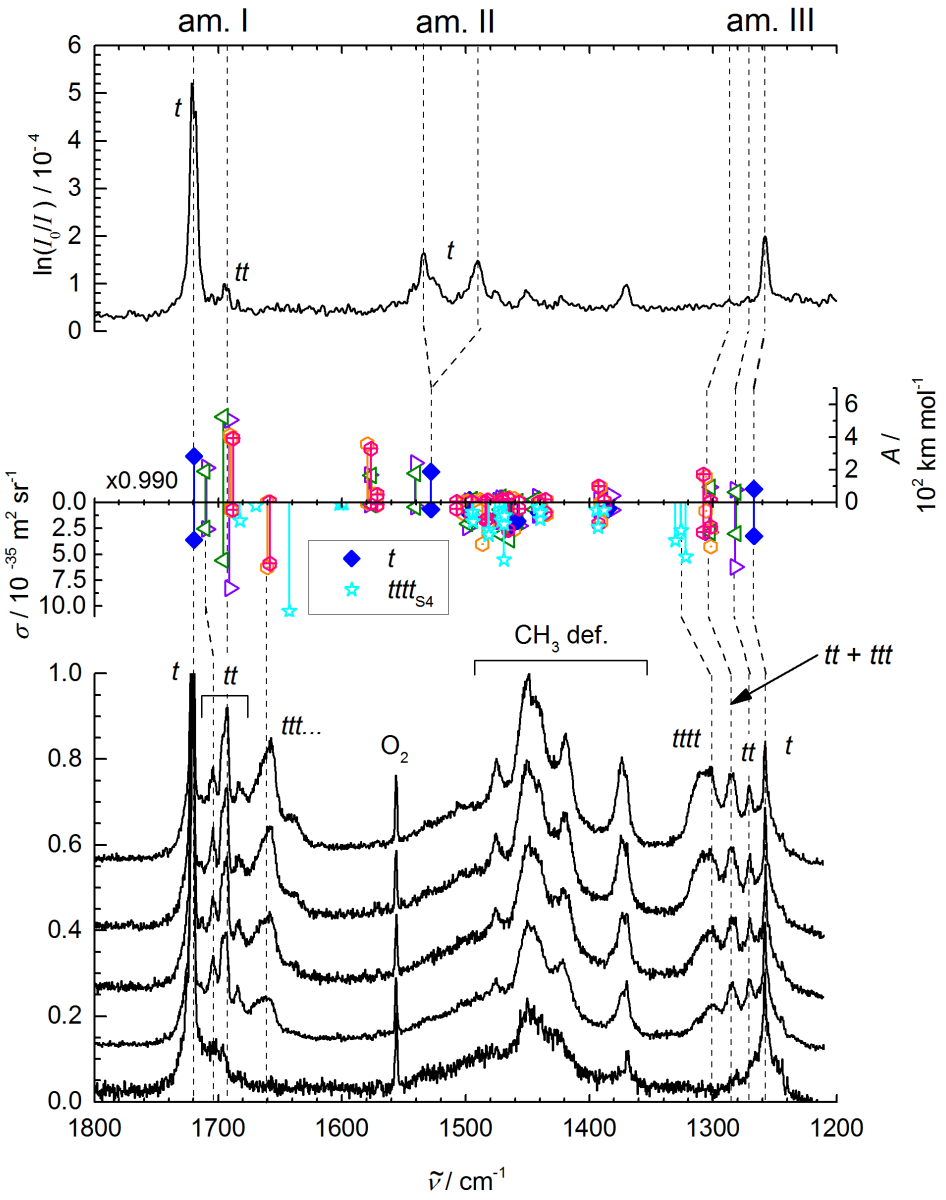

Fig. S5: Comparison of the experimental and harmonically predicted amide I–III and fingerprint spectra of NMA using IR (upper, highly diluted room temperature expansion) and Raman (lower, more concentrated expansions with progressive nozzle heating from top to bottom) spectroscopy. Harmonic stick simulations scaled to the correct monomer amide I transition at 1720 cm^{-1} are shown, pointing up for the IR band strength and down for the Raman scattering cross sections. Blue diamonds mark *trans*-NMA (the *cis* predictions differ, but are hardly visible in this spectral range), triangles the two dimer predictions (which do not differ significantly between the violet tt_C and the green tt_N isomer) and orange hexagons the ttt_a trimer predictions. Turquoise stars mark an exemplary cyclic tetramer structure. Impurity O_2 is marked in the spectrum and serves as an internal calibration aid. In the amide I and III regions, there are 2–3 relatively sharp dimer features shifted up/down in wavenumber from the monomer, respectively. At lower nozzle temperature, a broader trimer/larger cluster band appears, shifted further from the monomer, in both regions. The lowest wavenumber CH deformation band also shows a slight clustering shift. Relative scattering intensities suggest that the upper Raman spectra are cluster-dominated, whereas the lowest spectrum (which also has a lower concentration than the others) is clearly monomer dominated. We will come back to these spectra in a later publication.

Tab. S6: Experimental details of FTIR- and Raman spectra shown in Figs. 1 and 2. Temperatures are only provided for relative guidance, due to variations of laboratory temperatures and other conditions as well as gradients between sample and temperature probe.
Square brackets denote averages of two adjacent temperature runs (separated by nominal temperature differences of 10 °C) which were coadded for better signal-to-noise.

	Fig. 1	**Fig. 2 (top → down)**										
	FTIR	FTIR			Raman							
carrier gas pressure / bar	1.6	1.6			0.45							
saturator temperature / °C	22–24	25	20	15–20	60							
stagnation pressure / bar	0.75	0.75			0.45							
nozzle temperature / °C	24–27	26–30			70	80	90	90	100	[115]	[145]	[175]
probe time per cycle / s	0.1	0.1			420						420/504**	504**
cycle time* / s	35	25			420						420/504**	504**
no. of averaged cycles	1600	750	800	1600	16					32		
spectrometer aperture / mm	4.0	3.5			0.075							
slit dimension / mm^2	600 × 0.2	600 × 0.2			4.0 × 0.15							
transmission filter / µm	4.4–9.1	2.4–4.0			> 0.534							

*a cycle in the FTIR setup means 20 background-, two pre- and post-, as well as one probe scan at 80 kHz each (in total about 5 s) and waiting time for vacuum recovery. In the Raman setup, acquisition- and cycle time are the same due to negligible duration of shutter operation and data processing.
**changes in acquisition time due to significant laser power loss (25 W → 20 W).

Tab. S7: Band positions (rounded to integer cm^{-1}) of FTIR- and Raman measurements in Fig. 2 (top → down). All values are estimated peak centers rather than centroids of a fit function.

	FTIR			**Raman**							
t	3508	3508	3508	3508	3508	3508	3509	3509	3509	3508	3508
c	–	–	–	3469	3469	3469	3469	3470	3470	3469	3468
tt (high)	3395	3395	3394	3396	3396	3396	3396	3397	3397	3396	3395
ttt	–	–	–	3386	3385	–	–	–	–	–	–
tt (low)	3365	3365	3365	3367	3368	3367	3367	3367	3366	–	–

Tab. S8: Computed properties of *tt* NMA dimers engaging the acetyl lone pair (tt_{C}) or the amide lone pair (two isomers tt_{N} and $tt_{\mathrm{N'}}$ with different energies are predicted) of the acceptor C=O group in N−H hydrogen bonding, at the RI-B97D/TZVPP level (with D3 correction Ref. 1). N−H Stretching wavenumbers are obtained from scaled harmonic frequencies, either with a simple scaling factor taken to fit the monomer values (first line) or with a linear scaling factor fit on a series of peptide data (Ref 2). Calculations carried out with the TURBOMOLE package (Ref. 3). In contrast to the B3LYP predictions, the nearly isoenergetic tt_{C} and $tt_{\mathrm{N'}}$ isomers differ mainly in hydrogen bond distance and not in hydrogen bond angle, but this difference results in a similar wavenumber splitting as for B3LYP and experiment. This structural trend would be more consistent with a dispersion interpretation of the spectral difference between the isomers, rather than repulsion. Higher level structure optimizations than the ones presented in this work are invited.

Quantity \ Isomer	tt_{C}	tt_{N}	$tt_{\mathrm{N'}}$
$E_{\mathrm{r,el}}$ / $\mathrm{kJ \cdot mol^{-1}}$	0	1.7	0.1
$E_{\mathrm{r,0}}$ / $\mathrm{kJ \cdot mol^{-1}}$	0.3	1.9	0
d(H···O) / pm	200	207	204
α(H···O=C) / °	117	109	116
$\tilde{\nu}$(N−H) / $\mathrm{cm^{-1}}$	3353	3416	3386
SF 0.9816; fitted to monomer	3509	3511	3511
$\tilde{\nu}$(N−H) / $\mathrm{cm^{-1}}$	3339	3396	3370
- Linear SF fitted to peptide set[a]	3482	3484	3384
A_{IR} / $\mathrm{km \cdot mol^{-1}}$	524	212	238
	21	19	20

[a] $\tilde{\nu}_{\mathrm{scaled}}/\ \mathrm{cm^{-1}} = 0.89627\,\tilde{\nu}_{\mathrm{harmonic}} + 277.5$; Ref. 2

Tab. S9: Computed properties of *ttt* NMA trimers at the RI-B97D/TZVPP level (D3 correction). See Table 4 for notations and Table S8 for explanation of quantities.

Quantity \ Isomer	ttt_{a} 1→1'→2→1		ttt_{p}	ttt_{l} 1→2→3	
$E_{\mathrm{r,el}}$ / kJ · mol^{-1}	0		1.4	22.9	
$E_{\mathrm{r,0}}$ / kJ · mol^{-1}	0		1.6	17.8	
d(H···O) / pm	212	1→1'	214	192	1→2
	220	1'→2	214	192	2→3
	218	2→1	215	–	
α(H···O=C) / °	106	1→1'	107	115	1→2
	103	1'→2	108	119	2→3
	101	2→1	107	–	
$\tilde{\nu}$(N−H) / cm^{-1}	3399	1→1'	3402	3284[b]	1→2 & 2→3
SF 0.9816; fitted to monomer	3414	2→1	3411	3300[b]	1→2 & 2→3
	3423	1'→2	3414	3511	
$\tilde{\nu}$(N−H) / cm^{-1}	3380	1→1'	3382	3275[b]	1→2 & 2→3
Linear SF fitted to peptide set[a]	3394	2→1	3390	3289[b]	1→2 & 2→3
	3402	1'→2	3393	3482	
A_{IR} / km · mol^{-1}	97		6	995; sym.[b]	
	166		222	369; antisym.[b]	
	174		218	23	

[a] $\tilde{\nu}_{\mathrm{scaled}}$/ cm^{-1} = 0.89627 $\tilde{\nu}_{\mathrm{harmonic}}$ + 277.5; Ref. 2

[b] Symm. and antisymm. components of the coupled H-bonded N−H stretches

Tab. S10: Cartesian coordinates (in Å) of computed tt_C NMA dimer from B3LYP-D3(BJ)/aVTZ geometry optimizations in Gaussian 09 with convergence cutoffs set to 'tight' and integration grid to 'SuperFine'.

	$\boldsymbol{tt_C}$		
C	-2.4818321738	-0.3901150791	-0.2294838213
O	-3.6537995218	-0.3461520418	0.1239474146
N	-1.6655391671	0.6867147089	-0.1920522927
H	-0.6922348877	0.5895026983	-0.457474342
C	-1.8504104887	-1.6716870042	-0.7389120305
H	-0.818851113	-1.5401250555	-1.0603583824
H	-1.8963132122	-2.4222968638	0.050257217
H	-2.4434220558	-2.0426905751	-1.5736193285
C	-2.143536104	1.9715955799	0.2749901739
H	-2.5119595306	1.9075878681	1.3001296149
H	-1.3223007785	2.6835351235	0.2315894504
H	-2.9637863937	2.3345722915	-0.3453438483
C	1.8396786991	-0.1327706496	0.3140368406
O	1.2091947109	0.3511147266	-0.6230813819
N	3.1898834706	-0.1634165625	0.3074910102
H	3.6713987007	-0.5687985786	1.0889076956
C	1.1555876628	-0.7351789483	1.5186965766
H	1.8451896481	-0.9887066194	2.3218684098
H	0.4082000569	-0.0366540777	1.8891504919
H	0.628746089	-1.6369705742	1.207907277
C	3.9611397107	0.3618566377	-0.806457721
H	3.7207075444	-0.1684211473	-1.7273168717
H	3.7443804276	1.4182918948	-0.9596017994
H	5.0186613361	0.2403269879	-0.5875055826

Tab. S11: Cartesian coordinates (in Å) of computed tt_{N} NMA dimer from B3LYP-D3(BJ)/aVTZ geometry optimizations in Gaussian 09 with convergence cutoffs set to 'tight' and integration grid to 'SuperFine'.

	$\boldsymbol{tt_{\mathrm{N}}}$		
C	2.3193112968	-0.0137742712	-0.3002012219
O	1.3022179418	-0.1936264284	-0.9632733693
N	2.3196694401	-0.0823732564	1.0492887847
H	3.1784986237	0.0860316962	1.5401189809
C	3.6427621589	0.2953386151	-0.9597164047
H	4.461423886	0.4225476882	-0.2533628765
H	3.885420819	-0.5132408991	-1.6476303322
H	3.5336389098	1.2047750037	-1.548906371
C	1.1178801774	-0.3711682928	1.8146021858
H	0.6497501514	-1.2865926974	1.4576109417
H	1.3903519664	-0.4937398342	2.8593980656
H	0.3900750069	0.4344437375	1.728044548
C	-2.3041126783	0.5400989318	-0.0718527422
O	-3.4652675533	0.4458214112	0.3068916559
N	-1.5737657654	-0.527436052	-0.4641219617
H	-0.5986946672	-0.4056576516	-0.7056394937
C	-1.5905551768	1.8771897921	-0.1315873728
H	-0.5702843546	1.7998995296	-0.502450422
H	-2.1590292124	2.5449311648	-0.7776972966
H	-1.5865629566	2.3173698797	0.865591644
C	-2.1301719119	-1.8640235433	-0.4417876004
H	-2.3941624916	-2.1704145329	0.572605426
H	-3.0361607121	-1.9171227579	-1.0453552743
H	-1.3919218983	-2.5540132328	-0.8442444935

Tab. S12: Cartesian coordinates (in Å) of computed ttt_a NMA trimer from B3LYP-D3(BJ)/aVTZ geometry optimizations in Gaussian 09 with convergence cutoffs set to 'tight' and integration grid to 'SuperFine'.

	ttt_a		
C	5.971929448	2.7495508225	-4.1515493903
O	7.0830116879	2.9488281007	-4.6473676103
N	5.7594203846	2.7399310328	-2.8210764367
H	4.8910480344	2.3474981285	-2.4794330265
C	4.7463771192	2.5438932993	-5.0111351173
H	3.8723014331	2.2492730239	-4.4363393694
H	4.5369525397	3.4824785279	-5.5249343513
H	4.9584663682	1.796608268	-5.7717073609
C	6.8198068582	3.0205324754	-1.8737224266
H	7.4008235877	3.8725742017	-2.2192180336
H	6.3752425236	3.2540638889	-0.9092673378
H	7.5029780843	2.1784184097	-1.7526318928
C	7.5551363425	-0.633234688	-4.51892531
O	7.0857679863	-1.7645955157	-4.3802060059
N	7.3327900356	0.1153290694	-5.6174856379
H	7.55743986	1.1007487107	-5.5745355946
C	8.4617879881	-0.0112339751	-3.4832440235
H	8.5617126484	1.0640630096	-3.608198845
H	8.0855036453	-0.2383225836	-2.4894619989
H	9.4464714448	-0.471578224	-3.5752433451
C	6.5483278375	-0.3751665963	-6.7335689996
H	5.4790301862	-0.3850191855	-6.5139161596
H	6.7247644632	0.2652627778	-7.5942541382
H	6.8481431091	-1.392784532	-6.9735206478
C	4.192603846	-0.2946907702	-2.7888018679
O	3.6592272091	0.6914660552	-2.2759984397
N	5.215882413	-0.9495616199	-2.2049883738
H	5.7559421367	-1.592056188	-2.7700047445
C	3.708198893	-0.8832384206	-4.0931294606
H	4.4605698397	-1.5080539622	-4.5691447697
H	2.8278299522	-1.493014086	-3.8846067887
H	3.4040811306	-0.0834713275	-4.7624993123
C	5.7285948258	-0.5604270889	-0.9067711807
H	4.9034220968	-0.4156344755	-0.2126215142
H	6.3760033419	-1.3508273897	-0.5349764099
H	6.2966036995	0.3701018264	-0.9492990786

Tab. S13: Cartesian coordinates (in Å) of computed ttt_p NMA trimer from B3LYP-D3(BJ)/aVTZ geometry optimizations in Gaussian 09 with integration grid set to 'SuperFine'.

	ttt_p		
C	1.9310661316	0.9792631754	-0.5328145279
O	2.7170295353	0.036724144	-0.4123894621
N	1.4223300762	1.636906224	0.5271875519
H	0.6126072828	2.2274015106	0.3840660609
C	1.5158672378	1.5016371517	-1.8882839016
H	0.6868624739	2.2029118612	-1.8317738123
H	2.3757093757	2.0053778577	-2.3312855693
H	1.2577930705	0.6677717494	-2.5361649232
C	1.8194586018	1.3119838045	1.8821171096
H	2.9046568753	1.2644717853	1.9470786781
H	1.4537155658	2.0889264762	2.5488301518
H	1.4243170324	0.349912518	2.2098898209
C	-0.1799833367	-2.1603762703	-0.5188205171
O	-1.3660441006	-2.3729167935	-0.2566735789
N	0.7631815371	-2.0486427517	0.4366026077
H	1.655388743	-1.640647959	0.1870273158
C	0.3149101558	-2.0578691282	-1.9425932066
H	1.3353949903	-1.6880675618	-2.0065028173
H	0.2712204341	-3.0536037502	-2.3852559887
H	-0.3521472702	-1.4178653091	-2.5145160689
C	0.4472375665	-2.2342726021	1.8383190949
H	-0.1197815802	-3.1536581841	1.9702603054
H	1.3759732743	-2.3018525654	2.3993694137
H	-0.1497687421	-1.4149325937	2.2400516243
C	-1.8369851753	1.2334773973	-0.3012989854
O	-1.4020294784	2.3672340091	-0.0866957023
N	-2.0948446321	0.3581500905	0.6897313729
H	-2.2143690238	-0.6182706932	0.4507185651
C	-2.1614291005	0.7560784855	-1.6974991214
H	-2.3558161607	-0.3128251949	-1.7408609729
H	-3.0490832806	1.2910251011	-2.0369778691
H	-1.3475879984	1.0165535931	-2.369418651
C	-1.9329372169	0.7219648533	2.0827772518
H	-2.4294066554	1.6707220485	2.2766118738
H	-2.3833709271	-0.0513723472	2.6999880548
H	-0.8847512814	0.8320368683	2.3626338227

References

Ref. 1 : Grimme, S. ; Antony, J. ; Ehrlich, S. ; Krieg, H. ; A consistent and accurate ab initio parametrization of density functional dispersion correction (DFT-D) for the 94 elements H−Pu; *Journal of Chemical Physics* 132 (**2010**) 154104.

Ref. 2 : E. Gloaguen and M. Mons. Isolated neutral peptides. In A. M. Rijs and J. Oomens, editors, *Gas-Phase IR Spectroscopy and Structure of Biological Molecules*, volume 364, pages 225−270. Springer, Berlin, **2015**.

Ref. 3 : TURBOMOLE V6.3 **2011**, a development of University of Karlsruhe and Forschungszentrum Karlsruhe GmbH, **1989−2007**, TURBOMOLE GmbH, since **2007**.